Title:

Data registration for multi-method qualification of additive manufactured components

Authors:

M. Praniewicz[a*], G. Ameta[b], J. Fox[c], C. Saldana[a]

[a]Georgia Institute of Technology, 801 Ferst Drive, Atlanta, GA 30318

[b]Siemens Corporate Research, Princeton, NJ 08540

[c]National Institute of Standards and Technology[†], Gaithersburg, MD 20899

Abstract:

This work refines surface registration methods for metrological datasets to improve the multi-method qualification accuracy of additively manufactured (AM) lattices. Datasets acquired from X-ray computed tomography and a coordinate measurement machine of an AM lattice were aligned using derived geometry datum features based on a theoretical supplemental surface definition, which has been established in recent draft standards, but has had limited examination using complex AM structures. A refined sampling registration approach for lattice geometry based on spatially-dependent subsampling is derived and shown to statistically decrease variation between measurement sources. This importance of well-defined sampling practice and definition is highlighted. The applicability of this approach for multi-method qualification of complex AM parts is discussed. This work lays the foundation of utilizing specifications under consideration in a new standard with possible verification techniques that can be employed.

1 Introduction

Components manufactured using traditional processes (e.g., casting, forging) are often produced in large quantities. However, the cost of one-off and low volume components created using these processes is often extremely high due to investment in tooling. Additive manufacturing (AM) allows for the creation of such components with little additional capital expense, thus making it an extremely advantageous process for creating low-quantity complex components. However, qualification of components in industries that would greatly benefit from AM (e.g., aerospace, medical) is often laborious [1]. Moreover, non-destructive inspection of internal features becomes critical with low quantity components because of the greater cost percentage devoted to destructive testing. Because of this, the use of X-ray computed tomography (CT) has grown in popularity as an inspection method for these internal features [2]. While this method can yield promising results,

the true uncertainty of the measurement can be difficult to quantify as it changes with the measured geometry, material, and scan parameters [3-5]. Another option to validate measurements from CT is to pair them with conventional measurement techniques, such as coordinate measurement machines (CMM) or optical techniques [6-9]. While CT data is often expressed in the form of a boundary surface obtained from thresholding a voxel model, CMM data is delivered as a set of discrete points. By pairing the CT data with other measurements with well-defined uncertainties, techniques can be used to derive the uncertainty of the CT measurements [10]. Combining multiple measurements allows for a more complete digital reconstruction of the component [9]. A review of recent developments in metrology related to additive manufactured components is presented in [11].

One requirement for this analysis to take place is the registration of both data sets within a common coordinate system. For geometric qualification, this registration is correlated to the datum features defined in computer aided design (CAD) geometry or other manufacturing data. However, due to the complexity of geometries which can be created with AM, the definition of these datum structures may be challenging [12, 13]. Recently, new standards have been created to aid in the definition of this manufacturing data. The recently created ASME Y14.46 trial standard [14] puts forth (among other elements useful in product definition for AM) the notion of theoretical supplemental surfaces to specify the tolerance of lattice-based geometries. Designers can use supplemental surfaces to limit the variations in location, orientation, form and extent of overall lattice-based geometry using the techniques specified in the standard. Although, the specification was considered in the trial standard, no firm indications of verification were provided.

Building upon the initial specification in the ASME Y14.46 trial standard, previous work has investigated the use of these tools to specify and verify form variations of small triangular planar supplemental surfaces associated with a lattice structure [15]. However, no comparison against the nominal design geometry of the part was performed, as form (flatness) variation was compared with a plane. Data registration is also a crucial aspect when comparison with nominal design geometry is required. This is especially true when datum features are used to assign allowable variations. One of the simplest registration techniques using a datum hierarchy is commonly known as a 3-2-1 registration. Commonly used for datum alignment, this method sequentially constrains the six degrees of freedom of an object. This method can be executed simply by utilizing the minimum number of points for each feature (i.e., three for a plane, two for a line, and one for a point), or additional data points can be averaged to reduce the geometric uncertainty in the calculation of component features [16]. By using this method, a coordinate system can be fit to the data using a datum structure. By performing a registration of multiple data sets, the combination of these data sets can be used for comparison against a nominal model.

In this work, these new product definition standards are implemented to align and analyze an additively manufactured component using data from two different measurement methods: CMM and CT. The effect of data sampling used in registration is investigated. A refined sampling method for registration is then proposed and implemented. The effect of this refined sampling is then compared to the original alignment using parameters and statistical analysis.

2   Materials and Methods

2.1 Part / Datum / Measurand definition

The component analyzed in this work is a rectangular box comprised of a lattice with a uniformly patterned unit cell and an outer shell. The unit cell measures 5.08 mm per side and was patterned to make a 9 x 9 x 9 array. This CAD model was then sectioned in half along the Z direction to yield a total array of 45.72 mm x 45.27 mm x 22.8 mm in order to expose a half unit cell layer. A 2.54 mm thick wall was added to surround the lattice in the X & Y axes. A datum structure for the component was constructed, comprising of primary, secondary, and tertiary datum planes along the exterior of the component, labeled A, B, and C in Figure 1. The model was then exported from the CAD program as an .STL using a conversion tolerance of 0.001 mm.
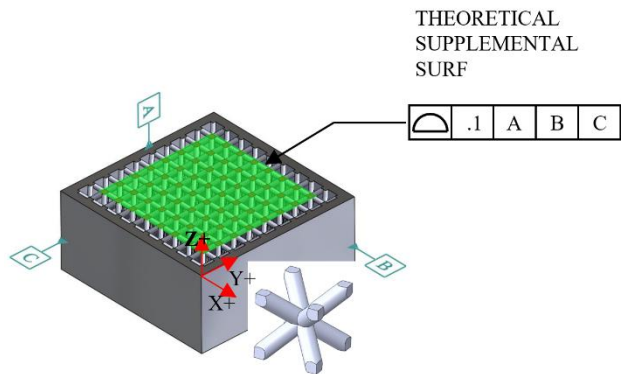

Figure 1: Nominal CAD design and lattice unit cell with specification per ASME Y14.46 trial standard

The measurand for this component was defined as the theoretical surface made up of the top nodes of the lattice, shown as the surfaces which intersect the theoretical supplemental surface (TSS) in Figure 1. These surfaces should ideally lie within the same plane as datum plane A. The form of each node surface, as well as the form of the theoretical surface formed by the combination of the individual measurand surfaces were evaluated, as detailed in section 3.

After the design was completed, the component was manufactured on an EOS Formiga P110 SLS machine out of EOS PA 2200 (nylon) using a layer height of 60 μm, the highest layer resolution possible for this system, and the manufacturer specified build parameters. The completed component can be seen in Figure 2.

2.2 Definition of measurement parameters

After manufacturing was complete the lattice component was qualified using both a CMM and CT. The CMM system used was a Zeiss Micura, with a calibrated maximum permissible error of length measurement ($E_{0,MPE}$) of $(.8 + L/400)$ μm. The datum surfaces were captured using a 3 mm diameter probe using a scanning strategy to capture points spaced 0.15 mm apart along the path traveling at 3 mm/s with a measurement force of 200 mN. The measurand data was captured using a 1.5 mm diameter stylus and used a 50 mN measurement force. These parameters were chosen based on results presented in Schild et al., where a small stylus and measurement force yielded the greatest agreement between tactile measurement and XCT measurement [7]. For each of the 64 measurand surfaces, measuring approximately 2.9 mm^2, 60 points were captured. The measurement setup, and the defined probing paths, are shown in Figure 2.
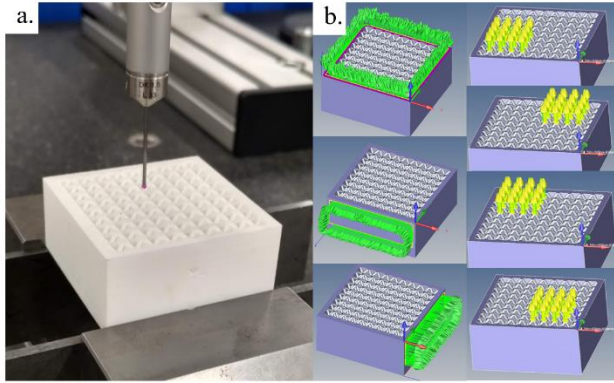
Figure 2: CMM measurement setup (a.) Example probing scenario (b.) Probing paths for the datum surfaces and measurand (split into four quadrants)

Computed tomography scans were completed on a 130 kV Zeiss Metrotom 800 and the setup can be seen in Figure 3 (a.). Parameters used in the scan can be found in Table 1.

Table 1: CT Scan Parameters

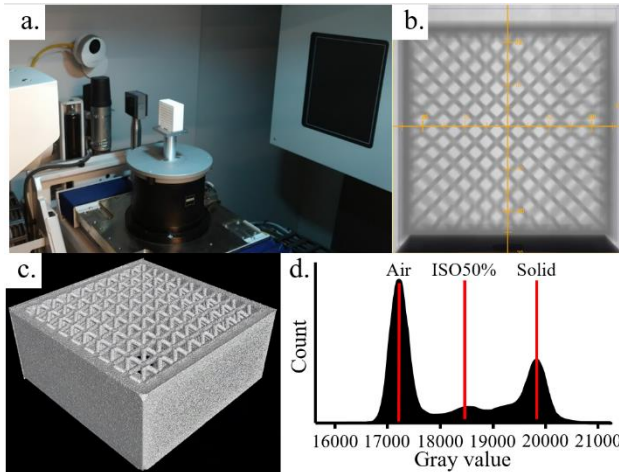| Parameter	Value
Voltage	90 kV
Current	83 μA
Number of Projections	1450
Integration Time	1 s
Source to Detector Distance	787.756 mm
Source to Object Distance	305.000 mm
Voxel Size	50.68 μm x 50.68 μm x 50.68 μm
Digital Filter	Shepp-Logan (High Pass)

Figure 3: (a.) Setup in CT system with (b.) single projection as well as (c.) the reconstructed surface image and (d.) histogram

The projections Figure 3 (b.) were then reconstructed using a Feldkamp algorithm [17]. The reconstructed volume was then imported into VGStudioMax 3.1 for thresholding. The component

surface was initially determined using ISO50 thresholding, then an advanced surface determination was completed within the software to determine the surface at a sub-voxel level using a deformable surface algorithm [18]. The thresholded model can be seen in Figure 3 (c.). After the component surface was determined, it was converted to a mesh using a meshing tolerance of 1 μm. Figure 3 (d.) shows the histogram of all XCT gray values.

3   Theory/Calculations

After the CMM and C3.T data were initially processed in their native environments, they were imported into MATLAB for registration and further analysis. The CMM data was imported as a list of discrete points, while the CT data was imported as an .STL file. Registration of the independent data sets was conducted using the datum planes in the component definition (Figure 1). The CMM data was first registered to the coordinate system within the CAD model using a 3-2-1 registration method using the prescribed datums in the product definition. The sets of measured points corresponding to the datum planes A, B, and C are denoted P_A, P_B, and P_C. First, a plane $\square_A$ was fit to the data P_A, using the least-squares method as described in [19]. The normal vector of $\square_A$ defines the primary axis in the data's local coordinate system $\hat{k}_1$. The centroid, or mean point, $\bar{p}_A$ of P_A was used as an arbitrary point on $\square_A$ for the following calculations. All points in P_B, were projected onto $\square_A$, resulting in a set of projected points P_B^*, as in Eq 1, 2;

$$\Delta = \hat{k}_1 \cdot (P_B - \bar{p}_A)^T \tag{1}$$

$$P_B^* = P_B - \Delta^T \hat{k}_1 \tag{2}$$

Δ is the distance from each point in P_B to $\bar{p}_A$ along $\hat{k}_1$. The projected points were then determined by subtracting the product of Δ and $\hat{k}_1$ from P_B. A line was fit to P_B^* via least-squares with the unit vector $\hat{i}_1$. The secondary datum is defined from $\hat{i}_1$ and a point p_B on the line. The final vector of the local coordinate system, $\hat{j}_1$, is given by the cross product of $\hat{i}_1$ and $\hat{k}_1$. The origin was then defined by first projecting P_C onto $\square_A$, yielding a set of points P_C^*. P_C^* was then projected on the secondary datum B, yielding the set of points P_C^{**}. The mean value $\overline{p_C^{**}}$ of P_C^{**} is the origin of the local coordinate system. The process for establishing this local coordinate system can also be seen graphically in Figure 4.
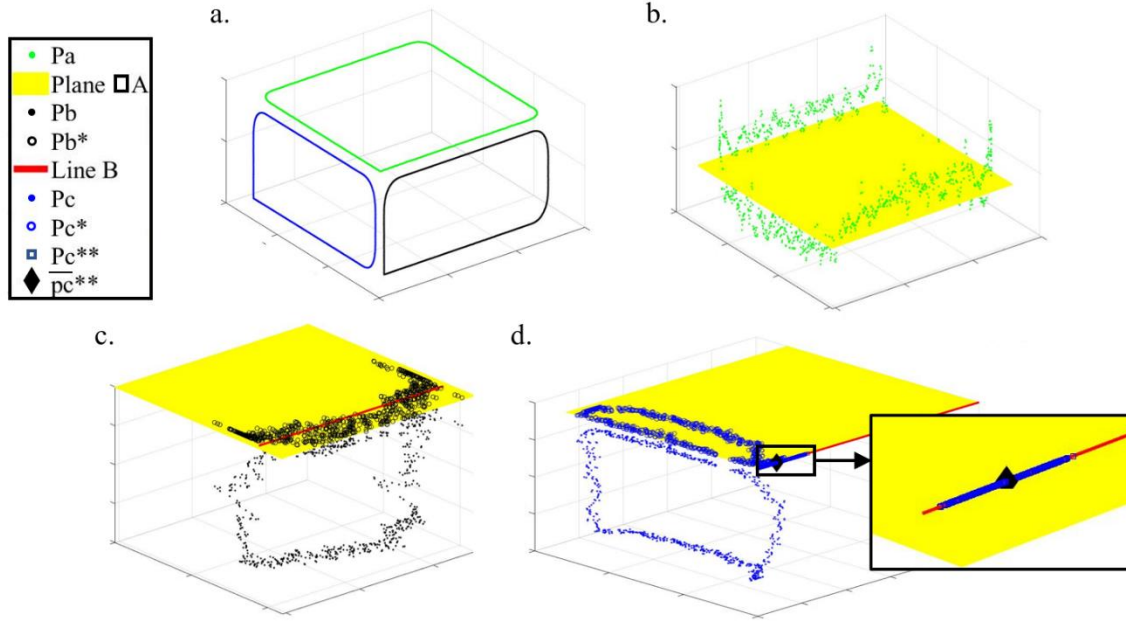
Figure 4: Visualization of coordinate system construction: (a.) Measured points P_A, P_B, and P_C, (b.) Construction of $\square_A$, (c.) Projection of P_B onto $\square_A$ and line B fit to P_B^* , (d.) Projection of P_C onto $\square_A$, projection of P_C^* and construction of $\overline{p_C^{**}}$

After the local coordinate system was established, the appropriate transformations, rotation R and translation $\overline{p_C^{**}}$, are required to align the local system with the part coordinate frame derived from CMM measurements. These registered points can be calculated as in Eq 3,4;

$$R = I[\hat{\imath}_l \quad \hat{\jmath}_l \quad \hat{k}_l]^{-1} \tag{3}$$

$$P_R = (RP^T)^T - \overline{p_C^{**}} \tag{4}$$

The final registered points, P_R, were then used in the analysis.
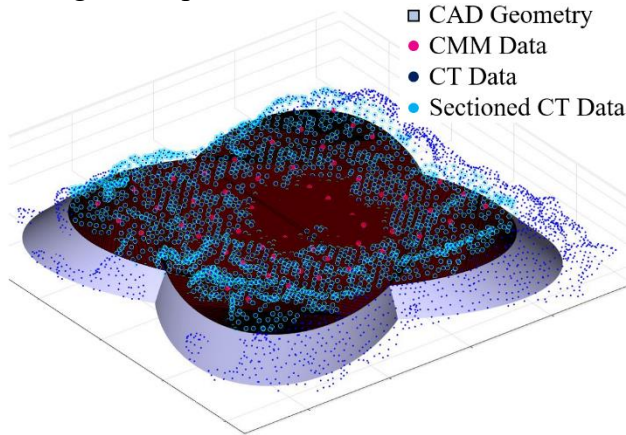

Figure 5: Example of measurand data segmentation for one measurand surface

This same registration process was also completed for the CT data, however the data sampled in the feature fitting process differed. While the CMM data contained discrete regions for each feature, the CT data is not divided into the subsequent features. User defined rectangular regions on the surface of the .STL were selected for each of the datum features. These regions were then used in the registration process.

After both data sets were registered in the same coordinate system, analysis of the measurand could occur. The data corresponding to each node was segmented by determining the points that lie within the normal projection of the top node surfaces, as shown as the light blue points in Figure 5. Two types of parameters were used to evaluate both data sets for each node: derived feature-based parameters and model deviation-based parameters. Ideally, the measurand should be planar based on the CAD geometry. For each node, plane features were fit using the previously described least squares algorithm and a Chebyshev algorithm for both the CMM and CT data [20]. The accuracy of least-squares algorithms used was verified using reference datasets from the NIST algorithm testing service [21]. The accuracy of the Chebyshev algorithm used was verified with a commercially available inspection software [22]. The alignment of the two data sets was analyzed by comparing the angle between the normal vector of the fit planes, θ, the Euclidean distance between the plane centers, δ, and the Z distance between the plane centers, δ_Z. These values were calculated using the following equations for the measurand surfaces, where N represents the total number of surfaces, v is the normal vector associated with the feature, p is the derived point on the plane, and a and b represent the two data sets:

$$\theta = \frac{1}{N} \sum_{i=1}^{N} \cos^{-1} \frac{v_{a,i} \cdot v_{b,i}}{|v_{a,i}||v_{b,i}|} \tag{5}$$

$$\delta = \frac{1}{N} \sum_{i=1}^{N} |p_{a,i} - p_{b,i}| \tag{6}$$

$$\delta_Z = \frac{1}{N} \sum_{i=1}^{N} p_{a,i,3} - p_{b,i,3} \tag{7}$$

These comparisons were completed for both types of fit planes. The deviation based parameters were calculated based on the distance of the data points from the nominal CAD geometry, and included the mean Δ, maximum Δ^+, minimum Δ^-, and standard deviation σ, of these distances. The projected distances for a region, α_i, can be calculated for a surface as in eq. 1. The parameters can then be calculated using α_i in the following equations:

$$\Delta = \frac{1}{N} \sum_{i=1}^{N} (\bar{a}_{a,i} - \bar{a}_{b,i}) \tag{8}$$

$$\Delta^+ = \frac{1}{N} \sum_{i=1}^{N} (\max a_{a,i} - \max a_{b,i}) \tag{9}$$

$$\Delta^- = \frac{1}{N} \sum_{i=1}^{N} (\min a_{a,i} - \min a_{b,i}) \tag{10}$$

$$\sigma = \frac{1}{N} \sum_{i=1}^{N} \left(\sqrt{\frac{1}{m} \sum_{j=1}^{m} (a_{a,i,j} - \bar{a}_{a,i})^2} - \sqrt{\frac{1}{l} \sum_{k=1}^{l} (a_{b,i,k} - \bar{a}_{b,i})^2} \right) \tag{11}$$

Rather than sampling the entire user defined region, better results could be achieved by selectively sampling the data used in this registration process. This is because of wide topology variations which can occur over the datum region (as seen in Figure 13). These will be explained in greater detail in the Discussion section. To improve the accuracy of this registration, a refined sampling registration was performed for the CT data set. In the previous technique, the data sampled from the full CT data set to define each of the datum features encompassed the entire region. In the refined registration, data is selectively sampled in areas that correspond to the areas sampled by the other data set. After initial registration has taken place, the primary datum feature is first analyzed. The algorithm iterates through the points of the datum feature in the CMM data set. For each point, a spherical region with radius R is created. The selection of R should be large enough to capture data from the XCT set despite inconsistencies which may arise from the original alignment, but small enough to not over sample. The data from the CT set that lies within the boundary of this sphere is sampled for the datum feature creation. This process continues through all points of the CMM datum, forming the sampled region of the CT data which can be used for primary datum creation. This process is repeated for the secondary and tertiary datum planes. After all data is sampled, registration can be performed as previously described. Figure 6 shows an example result of this sampling procedure and the resulting derived datum features.
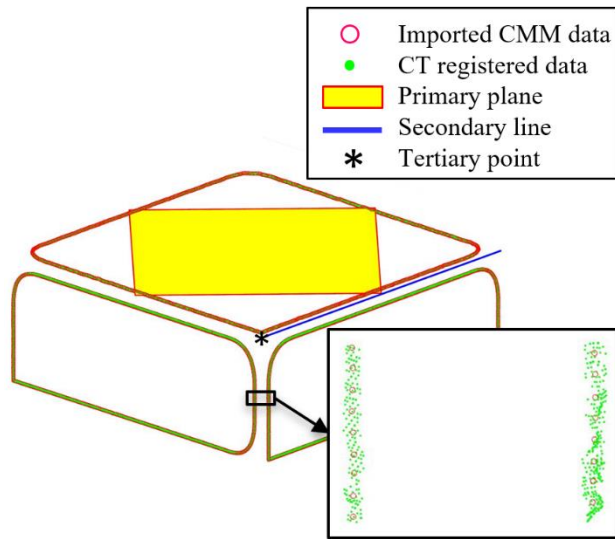

Figure 6: Example of refined sampling overall view, with inset detailing the sampled CT data and the corresponding CMM points

This refined registration method was compared against the initial registration using the previously described feature and deviation parameters to determine whether it is shown to significantly improve alignment between the two data sets.

4 Results

The results from the initial alignment of the two data sets were first considered. Figure 7 details the data obtained from the CT and CMM sets pertaining to one of the 64 surfaces and their corresponding fit planes. It can be seen that for the same node, four unique solutions for the same node surface are calculated. It is expected to see differences between the two fitting algorithms,

however variations also exist between the two data sets. Similar differences are observed to occur in the remaining measurand surfaces. The average results of the feature-based parameter comparison for all measurand surfaces are presented in Table 2.
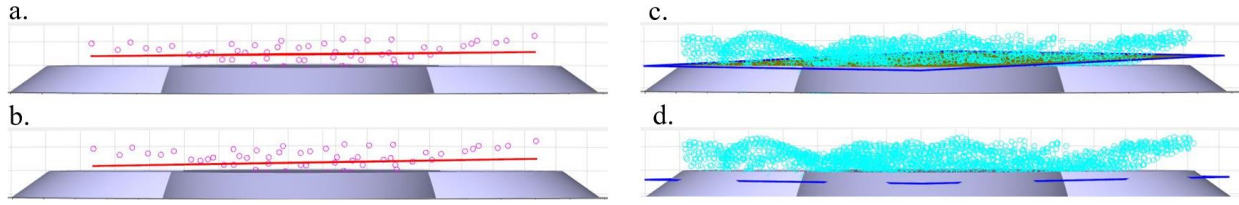

Figure 7: Feature fit results for initial alignment, node one: (a.) CMM least squares (b.) CMM Chebyshev (c.) CT least squares, (d.) CT Chebyshev

Table 2: Initial feature-based comparison between CMM and CT data

Least Squares Plane			Chebyshev Plane		
θ	δ	δ_Z	θ	δ	δ_Z
0.026 rad	0.141 mm	-0.045 mm	0.020 rad	1.061 mm	-0.062 mm

These results show that there are, on average, discrepancies in registration between the CT and CMM data. Some consistencies are shown between both plane fitting techniques. The average differences in orientation of the features seem to agree between the Least Squares and Chebyshev fitting, with θ's of 0.026 rad and 0.020 rad respectively. The δ_Z values have a lower Z value for the CT data than for the CMM data. However, the δ values shows a discrepancy of 0.92 mm. This is most likely due to the differences in the plane fitting algorithm. In the least-squares formulation, this point on the plane is the mean of all sampled points. In the Chebyshev formulation, the point on the plane is determined by the median location between the two minimum distance planes. Thus, in this case, while the Z values should be consistent, the X and Y locations of this point can vary significantly. Because of this, δ will not be reported for the remainder of the results.
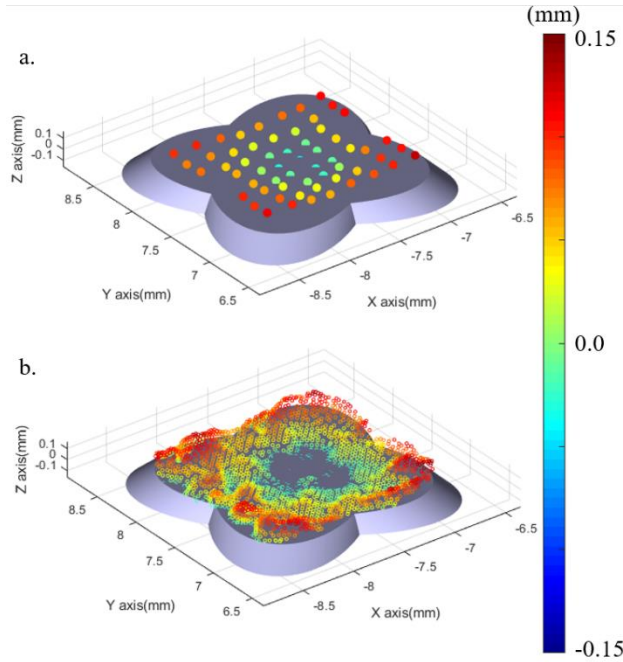
Figure 8: Surface deviation results for initial alignment, node one: (a.) CMM data (b.) CT data

Figure 8 shows the deviation results for node one, α_1. Similar trends in the surface topology are observed between the two data sets, showing the height of the surface decreasing towards the center of the node. The center of this node is shown to lie below the CAD model, meaning that the manufacturing process has not sufficiently met the product requirements. Because of the increased density of data, the CT data gives a much more detailed picture of the surface topology.

Table 3: Topology-based parameters for initial alignment

Δ	Δ^+	Δ^-	σ
0.046 mm	-0.017 mm	0.159 mm	-0.024 mm

Table 3 details the deviation-based parameters for all measurand surfaces of the initial alignment. The Δ parameter of 0.046 mm details that on average, the CMM data has a larger positive deviation from the CAD model than the CT data. This confirms the result shown in the δ_Z values of the feature-based parameters. Even with this offset in the data, the Δ^+ of -0.017 mm indicates that on average the maximum values in the CT are larger than the maximums of the CMM. Likewise, Δ^- of 0.159 mm indicates that on average, the lowest point of the CMM data has a larger Z value from the CAD surface than the CT data.

After analysis of the initial alignment was completed, the refined sampling registration was completed. Points were sampled from the CT data using the previously described sampling strategy with a radius of 0.1 mm. First, the feature-based parameters were compared in this alignment strategy compared to the initial. Figure 9 shows the fit features from the initial and refined alignment for measurand surface one. In both fitting algorithms for the features, we can

see a change in the location of the blue CT feature, indicating that there was a change in the overall alignment of the data.
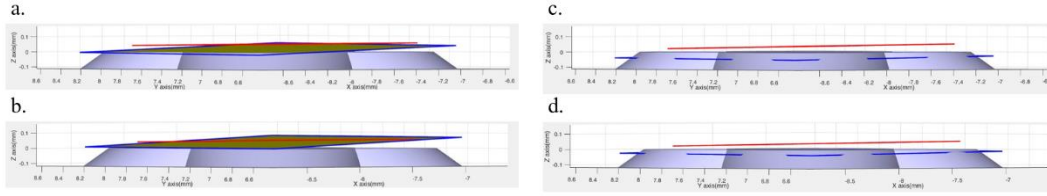

Figure 9: Feature based comparison, CMM plane(red) and CT plane (blue): (a.) Least squares with initial alignment, (b.) Least squares with refined alignment, (c.) Chebyshev with initial alignment, (d.) Chebyshev with refined alignment

The parameters for the feature-based comparison can be found in Table 4. The δ_Z and θ are presented for both alignments, as well as the standard deviation of the values in the individual measurand surfaces. On average, δ_Z has decreased in the refined alignment. However, little effect has occurred on θ. A two tailed T-test was conducted using a 95% confidence value with the null hypothesis stating that the original and refined means are equal. The critical T statistic for this case using the 64 sampled measurand surfaces was ≈ 1.97. After calculating the values for the data, it was shown that the refined sampling registration does show a significant effect for δ_Z for both plane fitting cases.

Table 4: Feature based parameters for initial/refined comparison

	Original mean	Original σ	Refined Mean	Refined σ	T stat	Test Result
LS θ	0.026	0.017	0.030	0.015	-1.35	Not Rejected
LS δ_Z	-0.046	0.014	-0.026	0.014	-7.95	Rejected
Cheb θ	0.020	0.012	0.020	0.009	-0.13	Not Rejected
Cheb δ_Z	-0.062	0.028	-0.052	0.025	-2.13	Rejected

The surface deviation results appear to reflect this as well, shown in Figure 10. The greatest change between (a.) and (b.) can be seen in the center of the measurand surface. In Figure 10 (a.), the CT data dips below the nominal surface significantly, while in Figure 10 (b.) the data appears shifted closer to the nominal surface, and more closely follows the CMM data. Because of this, the maximum values shown in the CT are exaggerated further. These maximum values lie close to the perimeter of the measurand surface and were observed because of the dense sampling in the CT data.
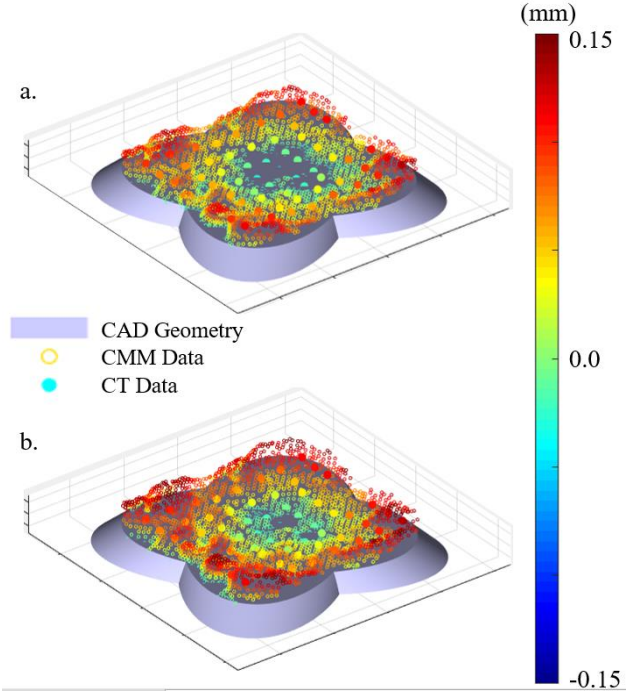
Figure 10: Surface deviation results for (a.) initial alignment and (b.) refined alignment

The deviation-based parameters for the original and refined alignment were compared as well, shown in Table 5. A T-test was again used to determine if there was a statistically significant change in any of the parameters. The Δ parameter shows a significant reduction, meaning that the mean deviation between the two data sets is closer together. This is expected based on the results seen in the feature-based parameters. Because of this, the average maximum difference, Δ^+, also has changed significantly from -0.017 mm to -0.026 mm. However, there is not a significant change observed in the average minimum difference, Δ^-. The authors believe this to be due minor shifts within the X,Y plane which occur in the refined registration. If a node is shifted slightly in X or Y, the data that is sampled relative to the CAD model will change. This may cause points along the edge of the node that slope into the lattice structure to be considered. While a few points would not have effect on the average, they could greatly affect the results of the minimum calculation.

Table 5: Feature based parameters for initial/refined comparison

	Original mean	Original σ	Refined Mean	Refined σ	T stat	Test Result
Δ	0.046	0.017	0.030	0.015	7.95	Rejected
Δ^+	-0.017	0.014	-0.026	0.014	6.32	Rejected
Δ^-	0.159	0.012	0.158	0.009	0.08	Not Rejected
σ	-0.024	0.028	-0.052	0.025	4.40	Rejected

The deviation between CMM and XCT was calculated by linearly interpolating the Z values of XCT data at the X,Y locations of the CMM data. The interpolated XCT Z values were then subtracted from the CMM Z values to calculate the deviation. Figure 11 (a.) shows this deviation for the initial alignment. The deviations calculated after the refined alignment are shown in Figure 11 (b.). The results presented appear to agree with the statistical analysis. The majority of points show positive deviations, shown as yellow to red coloration, in the initial alignment while the refined alignment shows the majority of points as light blue to green. Interestingly, one point is show in Figure 11 (b.) to increase in deviation, while it's neighbors appear to decrease. This could once again be attributed to shifting of the data in the X,Y plane during the registration process.
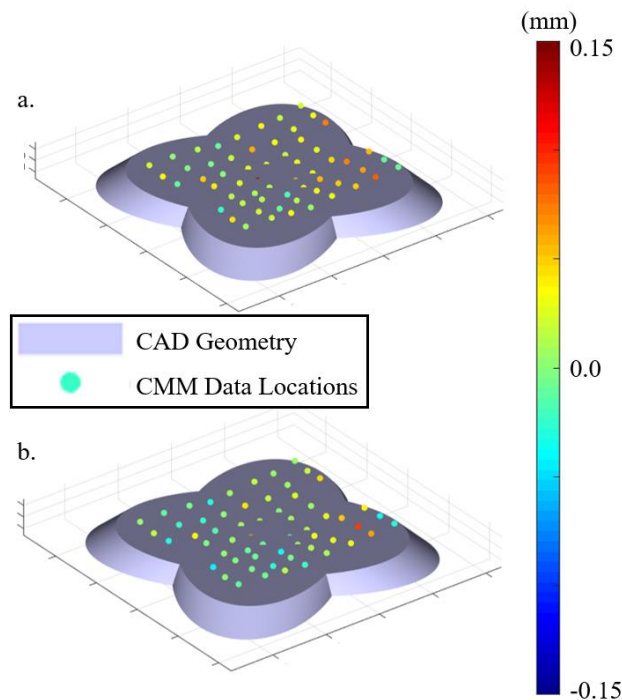

Figure 11: Deviation between CMM and XCT data (a.) initial alignment and (b.) refined alignment

5   Discussion

It is important to note the difference in the analysis performed in this work compared to that of the product definition provided in section 2.1. The analysis examined the change in feature and deviation-based parameters for the individual nodes in order to draw statistical conclusions for the overall effect. However, the specification designates a surface profile tolerance for the surface that the nodes lie within. This form measurement must be calculated by fitting a plane to all node data. This measurement was conducted as well in order to validate the measurements seen in the results section and to qualify the component.
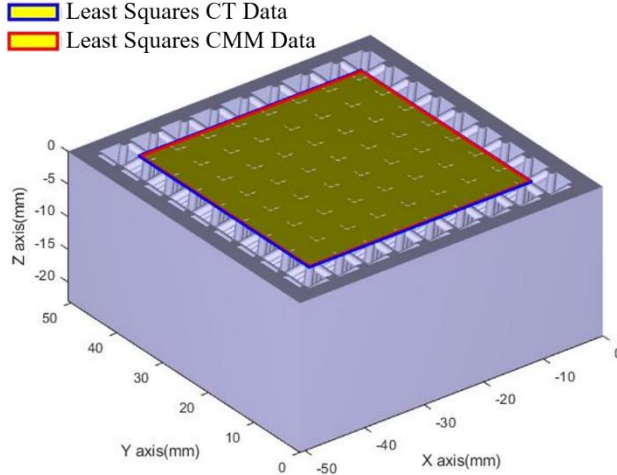
Figure 12: Measurement results for validation of TSS

Figure 12 demonstrates the least squares planes defined for each measurement method used in validation of the TSS. The differences in normal vector, mean position, form error, and residual error from fitting are compared between the two data sets. This was completed for the original alignment and the refined alignment. Differences between these two cases were also recorded. These results can be seen in Table 6. In the original alignment, differences between the feature fit to the CMM and CT data can be seen in all parameters, but most notably in the position, form and residual error. In the plane, we can see changes in all parameters. The difference in Z position between the two data sets is shown to be reduced, which agrees with the previously reported results. However, we can also see that the difference in form error between the two datasets increases as a result of the refined alignment. This is due to changes in points sampled as a result of the new alignment, and confirms the results seen in the deviation-based parameters. The new alignment may cause the edge points of nodes to be considered and effect the form measurement of the plane.

Table 6: Measurement results for overall plane fitting comparison

Data set	$\hat{i}$	$\hat{j}$	$\hat{k}$	x	y	z	Form	Residual
Original	-4.65E-05	-6.70E-05	3.28E-08	-4.92E-02	-2.90E-01	4.59E-02	1.43E-01	1.61E-02
Refined	-1.82E-04	-1.33E-04	9.16E-08	-7.20E-02	-2.67E-01	2.65E-02	1.51E-01	1.85E-02
Delta	-1.36E-04	-6.64E-05	5.88E-08	-2.29E-02	2.28E-02	-1.94E-02	7.30E-03	-.44E-03

In this work, significantly different results were observed using two different sampling methods to align CT and CMM data for the purpose of fully qualifying an additively manufactured component. The refined sampling method for registration was shown to align the data closer through reducing the deviation between the two data sets in both feature-based and deviation-based analysis. In the initial alignment, the entire datum surface of the part is sampled to create the CT primary datum. On closer inspection, this surface is not flat, and slopes up towards the edges. This can be seen as the yellow curve in Figure 13. If a line was fit to this data, one could expect this to be have a greater distance to the surface than the CMM contact point shown in the figure. However,

if one was to sample closer to the region inspected by the CMM, denoted by the two vertical lines, one could expect the result to be closer to that of the CMM.
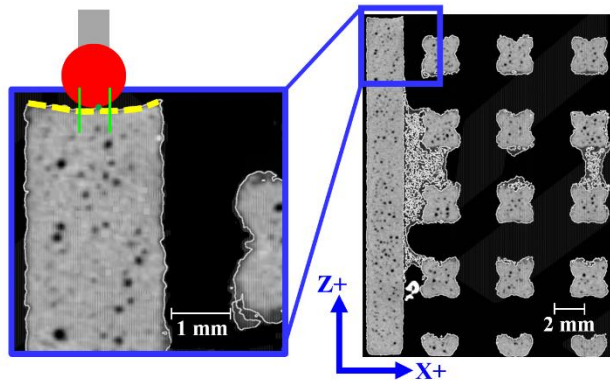

Figure 13: CT data image with CMM probing location

This illustrates the importance of sampling in the registration and evaluation of components created by AM. If this component was produced via a high precision manufacturing process, one could confidently make the assumption that this surface would closely resemble the ideal plane. However, in components produced by AM this assumption may not be accurate. Moreover, if the lattice structure itself were to be used as a datum, this assumption could stray even farther from reality due to the complexities associated with accurately creating fine features using AM.

An important caveat in this work is the construction of the coordinate systems used in the alignment procedure. On an ideal geometry and measurement procedure, this process would yield definitive results. However, for any physical object and measurement procedure, measurement with two different systems, or even repeated measurements with the same system, will create different coordinate systems. This is due to uncertainty and variation in the individual data points which propagates into the coordinate system construction. In the present study, this effect was not specifically examined, as the relative changes in alignment were of interest. Another point to note is that these components were measured in the as built condition. Because of this, the effects of surface roughness we be present in both measurement data sets. This roughness, and it's effect on data acquisition, have not been investigated in the present study. the A follow up study will investigate the construction of the individual part coordinate systems and estimation of their uncertainty.

6 Conclusion

In this work, a component was created via AM and qualified against specified product manufacturing data. The component consisted of a lattice and associated supplemental surface. The allowable variations and datum reference frame of the associated supplemental surface was specified using the conventions from ASME 14.46 trial standard. Two different techniques for verification of supplemental surfaces were explored. The component was measured by a CMM and CT to fully qualify the component geometry. These two datasets were then registered and compared using derived feature-based parameters and deviation-based parameters. A refined sampling technique was then used to improve the registration. The effect of this refinement was compared against the original registration using the defined parameters and statistical testing. It

was found that the refined registration improved the alignment between the two data sets. This work also highlights the importance of sampling in the registration and geometric qualification method of components produced by additive manufacturing. Moreover, this work demonstrates the importance of properly defining the procedure to sample data for evaluating the form of a TSS, which currently is not specified in the standard. This work lays the foundation for utilizing specifications under consideration in a new standard with possible verification techniques that can be employed. These verification techniques and related studies can then enable standards and practitioners to fully utilize the intent of such specifications. Future work will examine the registration of components where large flat datum surfaces are not available, such as lattice structures without supporting walls. The evaluation of the TSS in these cases becomes critical to the overall inspection plan.

Acknowledgement

References

[1] N. Kourra *et al.*, "Computed tomography metrological examination of additive manufactured acetabular hip prosthesis cups," (in English), *Additive Manufacturing,* vol. 22, pp. 146-152, Aug 2018.
[2] J. P. Kruth, M. Bartscher, S. Carmignato, R. Schmitt, L. De Chiffre, and A. Weckenmann, "Computed tomography for dimensional metrology," *CIRP Annals-Manufacturing Technology,* vol. 60, no. 2, pp. 821-842, 2011.
[3] W. Dewulf, K. Kiekens, Y. Tan, F. Welkenhuyzen, and J.-P. Kruth, "Uncertainty determination and quantification for dimensional measurements with industrial computed tomography," *CIRP Annals,* vol. 62, no. 1, pp. 535-538, 2013.
[4] M. Bartscher, U. Hilpert, J. Goebbels, and G. Weidemann, "Enhancement and proof of accuracy of industrial computed tomography (CT) measurements," *CIRP Annals-Manufacturing Technology,* vol. 56, no. 1, pp. 495-498, 2007.
[5] A. Cantatore and P. Müller, "Introduction to computed tomography," 2011.
[6] J. C. Fox, F. Kim, Z. Reese, and C. Evans, "Complementary use of optical metrology and X-ray computed tomography for surface finish and defect detection in laser powder bed fusion additive manufacturing," in *2018 ASPE and euspen Summer Topical Meeting-Advancing Precision in Additive Manufacturing*, 2018, vol. 69.
[7] L. Schild, A. Kraemer, D. Reiling, and H. Wu, "Influence of surface roughness on measurement uncertainty in Computed Tomography," presented at the 8th Conference on Industrial Computed Tomography (iCT 2018), Wels, Austria, 2018.
[8] F. Zanini, E. Sbettega, and S. Carmignato, "X-ray computed tomography for metal additive manufacturing: challenges and solutions for accuracy enhancement," *Procedia CIRP,* vol. 75, pp. 114-118, 2018.
[9] F. Zanini, E. Sbettega, M. Sorgato, and S. Carmignato, "New approach for verifying the accuracy of X-ray computed tomography measurements of surface topographies in additively manufactured metal parts," *Journal of Nondestructive Evaluation,* vol. 38, no. 1, p. 12, 2019.
[10] P. Muller, J. Hiller, Y. Dai, J. L. Andreasen, H. N. Hansen, and L. De Chiffre, "Estimation of measurement uncertainties in X-ray computed tomography metrology using the substitution method," (in English), *Cirp Journal of Manufacturing Science and Technology,* vol. 7, no. 3, pp. 222-232, 2014.
[11] R. Leach, D. Bourell, S. Carmignato, A. Donmez, N. Senin, and W. Dewulf, "Geometrical metrology for metal additive manufacturing," *CIRP Annals,* 2019.
[12] P. Witherell, J. Herron, and G. Ameta, "Towards Annotations and Product Definitions for Additive Manufacturing," (in English), *14th Cirp Cat 2016 - Cirp Conference on Computer Aided Tolerancing,* vol. 43, pp. 339-344, 2016.

[13] G. Ameta, R. Lipman, S. Moylan, and P. Witherell, "Investigating the Role of Geometric Dimensioning and Tolerancing in Additive Manufacturing," (in English), *Journal of Mechanical Design,* vol. 137, no. 11, p. 111401, Nov 2015.

[14] *ASME Y14.46-2017 Product Definition for Additive Manufacturing*, 2017.

[15] G. Ameta, J. Fox, and P. Witherell, "Tolerancing and Verification of Additive Manufactured Lattice with Supplemental Surfaces," *Procedia CIRP,* vol. 75, pp. 69-74, 2018.

[16] V. Bhat and E. C. De Meter, "An analysis of the effect of datum-establishment methods on the geometric errors of machined features," (in English), *International Journal of Machine Tools & Manufacture,* vol. 40, no. 13, pp. 1951-1975, Oct 2000.

[17] L. A. Feldkamp, L. C. Davis, and J. W. Kress, "Practical Cone-Beam Algorithm," (in English), *Journal of the Optical Society of America a-Optics Image Science and Vision,* vol. 1, no. 6, pp. 612-619, 1984.

[18] V. G. GmbH, " VGStudioMax 3.1."

[19] C. M. Shakarji, "Least-Squares Fitting Algorithms of the NIST Algorithm Testing System," *J Res Natl Inst Stand Technol,* vol. 103, no. 6, pp. 633-641, Nov-Dec 1998.

[20] C. M. Shakarji and A. Clement, "Reference algorithms for Chebyshev and one-sided data fitting for coordinate metrology," *CIRP Annals-Manufacturing Technology,* vol. 53, no. 1, pp. 439-442, 2004.

[21] "nist-l2-reference-pairs," ed. https://www.nist.gov/pml/sensor-science/dimensional-metrology/algorithm-testing: National Institute of Standards and Technology 2009.

[22] G. GmbH, "GOM Inspect 2017."